FILE & MAKE COPIES

AAS 91-164

# GP-B ORBIT MODELING AND INJECTION REQUIREMENTS

Penina Axelrad*, Richard H. Vassar†, and Bradford W. Parkinson‡

Gravity Probe B (GP-B) is a NASA spacecraft mission to test two previously unverified aspects of Einstein's theory of General Relativity. The plan is to measure two tiny drifts, known as the geodetic and frame dragging drifts, as manifested in a nearly perfect gyroscope in orbit around the Earth. Our goal is to measure these drifts to an accuracy of 0.4 marcsec/yr as compared to the direction to a distant inertial reference. Of this error, approximately 0.1 marcsec/yr is allocated to orbit induced drifts.

The ideal orbit for the GP-B spacecraft is circular, polar, and contains the line of sight to the guide star, Rigel. The drag compensation system employed to reduce the nongravitational disturbances acting on the science gyros governs the orbit motion during the course of the 18 month experiment. Thus, the orbit will be perturbed primarily by the non-central terms in the Earth's gravitational field, the Sun, and the Moon. An additional effect due to the precession of the equinoxes is also considered. These influences on the orbit are modeled and simulated in order to determine the initial orbit elements which will yield the smallest overall deviation from the ideal orbit. Injection error tolerances are derived to meet the desired Newtonian gyro drift rate of less than 0.1 marcsec/yr .

## INTRODUCTION

Gravity Probe B (GP-B) is a NASA project primarily designed to test two aspects of Einstein's theory of General Relativity. Based on General Relativity, L.I. Schiff predicted that a gyroscope in orbit around the Earth will undergo two motions not predicted by Newtonian analysis. These are known as the *geodetic* and *frame-dragging* precessions. In a precisely polar orbit at an altitude of approximately 650 km, the two effects would be orthogonal, with magnitudes of 6.6 arcsec/yr and 42 marcsec/yr, respectively. The GP-B spacecraft, planned to be launched in 1997, will carry extremely sensitive gyroscopes designed to measure these relativity effects to an accuracy of three tenths of a milliarcsecond (0.3 marcsec) or better. The history of the program development, which began about 1963, and the technology applied to solving the problems associated with measuring the relativity effects are described in references such as Everitt [*1980*].

---

* Dr. Axelrad is a Member of the Technical Staff at Stanford Telecom in Santa Clara, CA. This work was performed while she was a Research Assistant at Stanford University.

† Dr. Vassar is a Research Scientist at the Lockheed Research Labs in Palo Alto, CA.

‡ Prof. Parkinson holds a joint appointment in the departments of Aeronautics and Astronautics and the Hansen Experimental Physics Lab at Stanford University. He is the Program Manager for the GP-B project.

Every effort is taken to reduce disturbances which would cause Newtonian drifts of the gyroscopes in order to achieve this unprecedented level of accuracy. The experimental package has been carefully designed making use of cryogenics and superconductivity to create a stable, disturbance-free environment. The relativity gyros are quartz spheres coated with superconducting niobium, electrostatically supported inside a quartz housing. The entire cryogenically cooled experimental package is carried on a "drag-free" satellite which uses proportional helium thrusters to counteract all nongravitational forces acting on the spacecraft. Each of the four gyros is spun up so that its axis is initially aligned with the line of sight to the star Rigel to within a few arcseconds.

The direction to Rigel serves as a "distant inertial" reference against which the relativity drifts are to be compared. A telescope mounted along the vehicle axis of symmetry senses the apparent position of the guide star. The pointing control system will keep the spacecraft aligned toward this image to within 20 marcsec [*Parkinson and Kasdin, 1988*]. Over the course of the experiment, the star image will move due to both the physical drift of the star, known as proper motion, and optical effects such as parallax, deflection of starlight, and annual aberration. All of these effects are well known and can be reliably calibrated and removed in the data reduction.

The most difficult errors to correct are Newtonian drifts of the gyros. These drifts would be caused by forces exerted by the suspension system on the *nearly* spherical gyros. The spacecraft has been designed so that most of these forces will average to zero over an orbit or over the 10 minute roll period. However, if the spacecraft symmetry axis does not lie in the orbit plane, gravity gradient torques on the spacecraft will not average to zero, and there will be a net support force exerted on the gyros. Such a misalignment will occur for two reasons: 1) the spacecraft must rotate to track the apparent motion of the star, and 2) the orbit plane will rotate due to perturbing gravitational forces. The largest contributor to the spacecraft rotation is the 20 arcsec annual aberration which must be tracked. Further background information on GP-B can be found in references such as Parkinson et al. [*1986, 1987*].

The primary drivers in the selection of an appropriate orbit for the GP-B spacecraft mission are minimization of torques from nongravitational forces on the science gyros, separation of the geodetic and frame-dragging effects, and maximization of the relativity and geodesy data signals. This translates into an ideal orbit which is circular, polar, and contains the line of sight to the guide star, Rigel. Nongravitational disturbances on the orbit during the science mission are reduced to less than $10^{-10}$ g's through the use of a drag compensation system; however, this precludes any type of orbit adjustments to maintain the nominal orbit. There are three major ramifications: 1) orbit corrections can *only* be performed prior to the start of science data collection, 2) the ideal orbit can only be achieved in an average sense, and 3) the target injection orbit must be determined very accurately, accounting for the deviations which will occur over the course of the mission. Clearly, *a priori* modeling of the GP-B orbit is critical.

This paper focuses on the modeling of the GP-B orbit, and the derivation of orbit injection accuracies necessary to achieve the goal of Newtonian gyro drifts of less than 0.1 marcsec/yr. The first section below provides background on the the orbit requirements. Variational equations are then given for the set of orbit elements used to describe the GP-B

orbit. The following sections develop the models of the perturbations caused by the Earth's noncentral gravitational field, the Sun and Moon gravity gradients, and the precession of the equinoxes. Numerical simulation results are presented to show the orbit variations over the course of the 18 month GP-B science mission, and the preliminary orbit injection requirements derived from these simulations, are summarized.

## ORBIT REQUIREMENTS

The parameters of the spacecraft orbit influence both the relativistic drift and the Newtonian precession of the science gyros. The ideal orbit is circular, polar, and contains the line of sight to Rigel. If such an orbit could be achieved, it would have the following advantages.*

1. Gravity gradient torques on the gyros average to zero over an orbit.
2. Suspension torques on the gyros average to zero over an orbit.
3. Geodetic and frame-dragging effects are orthogonal.
4. Data reduction is simplified.

If the orbit is nearly circular, it has the added benefit of obtaining the minimum average altitude for a given dewar size.

Of course, it is impossible to maintain or even to inject the spacecraft into the nominal orbit perfectly. Thus there will be precessions of the science gyros other than the northerly geodetic and the eastwardly frame-dragging drifts. There are two ways to deal with these disturbances to the relativity signals. The first is to try to reduce the disturbance to an acceptably small level. If this is not possible, the second approach is to account for the disturbance by mathematically modeling it in the data reduction. In practice it is likely that a combination of these methods will be employed. The current goal is to reduce the physical error in the frame-dragging drift to 1% of the expected value, i.e. 0.4 marcsec/yr. Of this we allocate about 0.1 marcsec/yr to errors caused by orbital effects. In the following paragraphs the contributions to the measured science gyro drifts due to orbit deviations from the nominal are summarized and possible calibration methods are briefly discussed. The general recommendation is that deviations from the ideal orbit plane should be reduced to the lowest level possible.

### Relativity Drifts

The orbit averaged geodetic and frame-dragging drift rates were given by Everitt [*1980*] as follows:

$$\begin{aligned} \dot{s}_G &= A_G \left(\cos i \cos \delta_R - \sin i \sin \delta_R \sin \Omega\right) \hat{E} + A_G \sin i \cos \Omega \hat{N} \\ \dot{s}_{FD} &= -\frac{1}{2} A_{FD} \left[\left(1 + 3 \cos 2i\right) \cos \delta_R - 3 \sin 2i \sin \delta_R \sin \Omega\right] \hat{E} \\ &\quad -\frac{3}{2} A_{FD} \sin 2i \cos \delta_R \hat{N} \end{aligned} \tag{1}$$

* These advantages are only approximate. That is, given the ideal orbit, the Newtonian torques on the gyros will *approximately* average to zero. Further discussion of this can be found in Keiser [ *1985*].

where the relativity drift constants, $A_G$ and $A_{FD}$, are,

$$A_G = \frac{3}{2}\frac{\mu_E\, n}{c^2 a(1-e^2)}, \quad A_{FD} = \frac{G\, I_E\, \omega_E}{2\, c^2 a^3 (1-e^2)^{3/2}} \tag{2}$$

and $\mu_E$ is the Earth's gravitational constant, $n$ is the orbit rate, $c$ is the speed of light, $a$ and $e$ are the semimajor axis and eccentricity of the orbit, and $\omega_E$ is the Earth's rotation rate.

For a 650 km circular orbit the computed values of $A_G$ and $A_{FD}\ cos\ \delta_R$, are 6.6 arcsec and 42 milliarcsec per year respectively [*GP-B, 1988*]. Notice that these coefficients would become smaller if the semimajor axis, $a$, were increased.

By making approximations for small values of $i'$ and $\Omega$, Eq. 1 becomes,

$$\begin{aligned} \dot{s}_G &= A_G\ (i'\ cos\ \delta_R\ -\ \Omega\ sin\ \delta_R\ )\hat{E} + A_G\ \hat{N} \\ \dot{s}_{FD} &= A_{FD}\ cos\ \delta_R\ \hat{E}\ -\ A_{FD}\ 3\ i'\ cos\ \delta_R\ \hat{N} \end{aligned} \tag{3}$$

Thus the geodetic signal appears primarily in the north direction, whereas the frame dragging drift is primarily easterly. Since $A_G$ is two orders of magnitude larger than $A_{FD}$, we should compare the eastward component of the geodetic drift to the primary frame dragging term. Substituting the right ascension and declination of Rigel into Eq. 3 gives,

$$\dot{s}_{G_{East}} \approx A_G (i' - 0.15\,\Omega) \tag{4}$$

In order to separate this term from the frame-dragging drift, we must know the values of the coinclination and node of the orbit to better than about $10^{-3}$ deg (125 m). The eastward component of the geodetic drift can be determined by first obtaining the geodetic coefficient based on the northward drift alone (the northward frame-dragging drift is negligible). The frame-dragging term is then isolated by estimating and removing the eastward geodetic drift based on the estimate of $A_G$ and the time history of the inclination and node.

Newtonian Precessions

Vassar [*1982b, 1986*] identified and modeled the orbit dependent torques and the resulting Newtonian precessions of the gyroscopes as part of an end to end error analysis of the relativity mission. The most significant drifts are caused by torques produced by the gyro suspension system acting on the nearly perfect gyros. The suspension system keeps each of the science gyroscopes centered within the housing and supports it against residual specific forces including gravity gradients due to the separation of the gyro from the proof mass, centrifugal acceleration due to spacecraft roll, random drag, and disturbances caused by the pointing system.

Vassar found that the largest contribution was due to the gravity gradient forces, and computed the resulting gyro drift rates to first order in the angle between the gyro spin axis and the orbit plane ($\gamma$). This angle is given by the following combination of the orbit coinclination ($i'$) and node measured relative to Rigel ($\Omega$) [*Vassar, 1986*].

$$\gamma \equiv i' \sin \delta_R + \Omega \cos \delta_R \tag{5}$$

Gyro drifts due to both primary suspension torques caused by the interaction of the support forces counteracting the gravity gradient force with the gyro out of roundness, and the secondary suspension torques due to the asphericity of the gyro and the asphericity of its housing were considered. The rotor shape is modeled by a spherical harmonic expansion similar to the model of the Earth's graviational field. Vassar found the dominant component to be the primary torque due to the even terms in the harmonic expansion which produces a northward drift of approximately 500 $\gamma$ marcsec/ yr, where $\gamma$ is measured in radians. Thus

$$\dot{s}_{gg} \approx 500 \, ( \, i' \sin \delta_R + \Omega \cos \delta_R \, ) \; marcsec/yr \tag{6}$$

This expression can be integrated using the results of long term simulations of the variations of the orbit plane to determine if the Newtonian drrateift will be within the desired error margin of 0.1 marcsec/yr. In the simulation results it will be shown that this goal ***can*** be achieved if highly precise orbit injection requirements are met.

The suggestion has been made that if the Newtonian drift is in fact significant, it would be possible to calibrate it in the data reduction based on the orbit plane time history. There are several difficulties which might arise in trying to carry out this scheme. For example, the effects of capacitance differences, gyro mis-centering, drifts in the suspension system null, and thermal gradients would be impossible to model and calibrate. It may be possible to extract from the measured data enough information to determine coefficients describing the mean shape of the gyroscopes using techniques developed by Feteih [*1990*], and Cohen [*1990*]. However this would add complications to an already difficult data reduction task.

Altitude Variations

The requirement for the GP-B spacecraft to be placed in a nearly circular orbit is based on two objectives - to make the eccentricity small enough that second order terms can be ignored, and to keep the average orbit altitude as low as possible so as to maximize the relativistic drifts. In order for the spacecraft to remain drag free, the translational control system must have sufficient control authority to compensate for the maximum atmospheric drag, which generally occurs at the perigee of the orbit. Since the perigee altitude is set by the helium vent rate of the dewar, the minimum average semimajor axis would be achieved by a circular orbit. Unfortunately, the combination of the Earth oblateness and odd harmonic terms, cause even an initially circular orbit to become elliptical. Periodic altitude variations of 15 km, corresponding to a maximum eccentricity of 0.002, are acceptable since it produces only a minimal reduction in the relativistic drifts.

## ORBIT PERTURBATION EQUATIONS

Disturbances can produce both secular and periodic variations in the spacecraft instantaneous orbit elements. In this paper we address only the long term motions; thus all effects are averaged over an orbit and disturbances which produce only short term periodic

oscillations of the instantaneous elements are not included in the analysis and simulations. However, to determine the precise instantaneous target injection values for a given date and time, these periodic variations must be added to the mean target values discussed here. For example, for a near polar orbit, the $J_{2,2}$ term in the Earth's Gravitational field causes the instantaneous inclination to oscillate about a mean value with an amplitude of 0.002 deg and a twice daily period. Similar variations occur in the ascending node. The in plane elements oscillate with fairly large amplitude, at the orbit frequency due to perturbations produced by the Earth oblateness. Except where otherwise noted, all elements refer to the daily mean values.

Fig.1 shows the orbit elements used to describe the GP-B orbit. They are similar to the Delaunay and the equinoctial elements often mentioned in the literature [*Battin, 1987*]. The semimajor axis, $a$, and right ascension of the ascending node, $\Omega$, in this case referred to Rigel, are two of the classical elements. The coinclination, $i' = \frac{\pi}{2} - i$ is substituted for the inclination, $i$, to facilitate small angle approximations for the near polar orbit. Because the orbit is nearly circular, the argument of perigee ($\omega$) and true anomaly ($f$) are poorly defined. The components of the eccentricity vector in the equatorial plane, $\xi$, and in the northward direction, $\eta$, and either the argument of latitude, $u$, or the mean argument of latitude, $u_0$, are used instead of $e$, $\omega$, and $f$.

$$\xi = e \cos\omega , \quad \eta = e \sin\omega , \quad u = f + \omega \quad or \quad u_0 = M + \omega \tag{7}$$

Disturbing forces exerted on the GP-B spacecraft cause its orbit to deviate from a Keplerian ellipse. For a typical near Earth spacecraft these disturbances are primarily due to atmospheric drag, solar radiation pressure, noncentral terms in the gravitational field of the Earth, amd gravity gradients of the Sun and the Moon. GP-B is unusual in that the drag compensation system will eliminate the atmospheric drag and solar pressure effects on the orbit down to a level of less than $10^{-10}$ g's. Other orbit perturbations which must be considered are solid Earth tides, and precession of the equinoxes.

The effects of these disturbances on the orbit elements can be analyzed using standard variational methods, expressed in terms of either a perturbing potential or force.

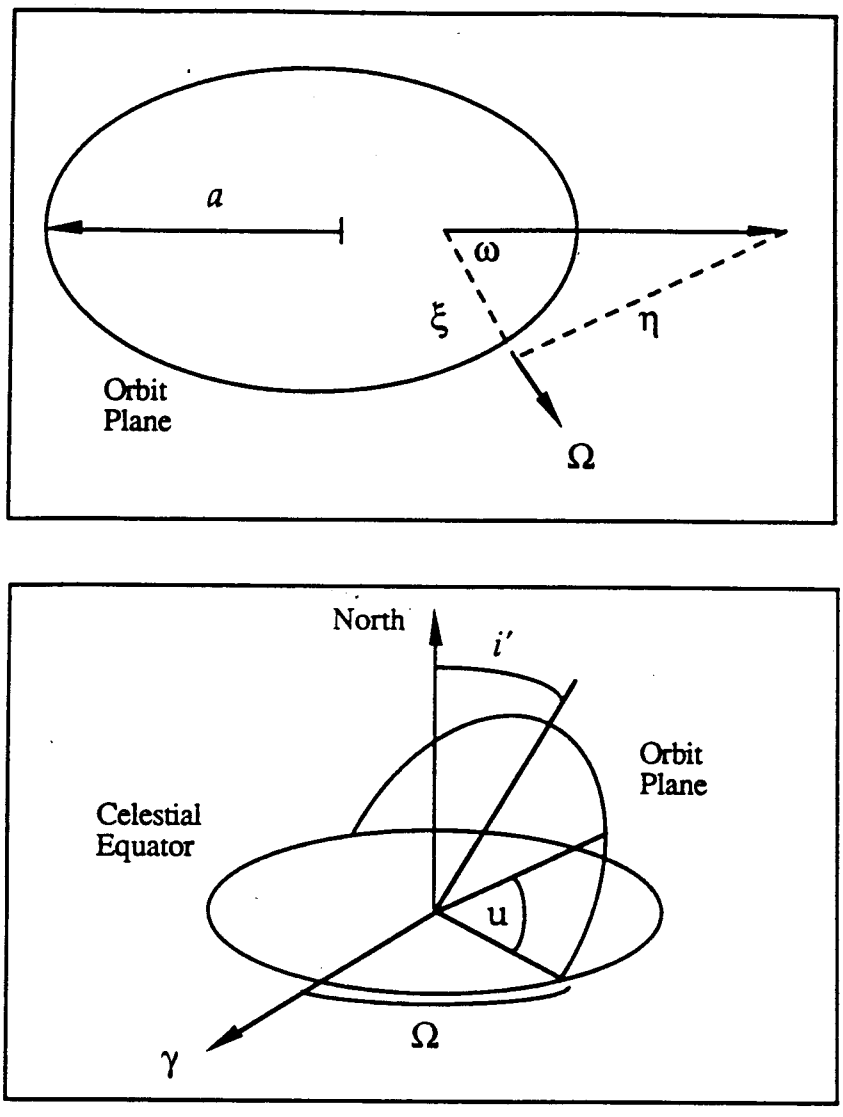


$a$ - semimajor axis

$\xi = e \cos \omega$ - component of e vector in equatorial plane

$\eta = e \sin \omega$ - component of e vector orthogonal to equatorial plane

$i'$ - coinclination

$\Omega$ - right ascension of the ascending node

$u$ - argument of latitude

**Fig. 1 Definition of Orbit Elements for GP-B.**

*Eliminates singularities of classical elements for a polar, near circular orbit.*

The variational equations for the orbit elements in terms of a disturbing potential are given by,

$$
\begin{aligned}
\frac{da}{dt} &= 2\sqrt{\frac{a}{\mu_E}}\,\frac{\partial U}{\partial u_0} \\
\frac{d\xi}{dt} &= -\frac{\gamma}{\sqrt{\mu_E a}}\,\frac{\partial U}{\partial \eta} - \frac{\gamma\,\xi}{(1+\gamma)\sqrt{\mu_E a}}\,\frac{\partial U}{\partial u_0} - \frac{\tan i'\,\eta}{\gamma\sqrt{\mu_E a}}\,\frac{\partial U}{\partial i'} \\
\frac{d\eta}{dt} &= \frac{\gamma}{\sqrt{\mu_E a}}\,\frac{\partial U}{\partial \xi} - \frac{\gamma\,\eta}{(1+\gamma)\sqrt{\mu_E a}}\,\frac{\partial U}{\partial u_0} + \frac{\tan i'\,\xi}{\gamma\sqrt{\mu_E a}}\,\frac{\partial U}{\partial i'} \\
\frac{du_0}{dt} &= \sqrt{\frac{\mu_E}{a^3}} - 2\sqrt{\frac{a}{\mu_E}}\,\frac{\partial U}{\partial a} + \frac{\gamma\,\xi}{(1+\gamma)\sqrt{\mu_E a}}\,\frac{\partial U}{\partial \xi} + \frac{\gamma\,\eta}{(1+\gamma)\sqrt{\mu_E a}}\,\frac{\partial U}{\partial \eta} + \frac{\tan i'}{\gamma\sqrt{\mu_E a}}\,\frac{\partial U}{\partial i'} \\
\frac{di'}{dt} &= \frac{\tan i'\,\eta}{\gamma\sqrt{\mu_E a}}\,\frac{\partial U}{\partial \xi} - \frac{\tan i'\,\xi}{\gamma\sqrt{\mu_E a}}\,\frac{\partial U}{\partial \eta} - \frac{\tan i'}{\gamma\sqrt{\mu_E a}}\,\frac{\partial U}{\partial u_0} + \frac{1}{\gamma\sqrt{\mu_E a}\cos i'}\,\frac{\partial U}{\partial \Omega} \\
\frac{d\Omega}{dt} &= -\frac{1}{\gamma\sqrt{\mu_E a}\cos i'}\,\frac{\partial U}{\partial i'}
\end{aligned}
\tag{8}
$$

where $\gamma^2 = 1-e^2$.

The potential form of the variational equations is particularly useful because there is no explicit dependence on the time variable, $u_0$. Thus to determine to first order, the average rate of change of the elements, we need only average the potential, $U$, and compute the rates using Eq. 8.

## Earth Harmonics

In this section the disturbance to the orbit due to the nonspherical gravitational potential is considered. The Earth oblateness, sometimes referred to as $J_2$, has the most significant effect on both the orbit plane and the evolution of the eccentricity vector. Various tesseral terms have periodic effects on the orbit, but no significant near resonances were found for the suggested choice of orbit altitude (650 km).

The spherical harmonic expansion of the perturbing geopotential is given by Kaula [*1966*] as,

$$U_E = \sum_{l=2}^{\infty}\sum_{m=0}^{l} U_{lm} = \sum_{l=2}^{\infty}\sum_{m=0}^{l} \frac{\mu_E R_E^l}{r^{l+1}}\left[C_{lm}\cos m\lambda + S_{lm}\sin m\lambda\right] P_{lm}(\sin\phi) \tag{9}$$

where $C_{lm}$ and $S_{lm}$ are empirically determined coefficients, and $P_{lm}$ are the associated Legendre Functions. The coefficients are often normalized for computation purposes.

$$\overline{C}_{lm} = \left[\frac{(l+m)!}{(l-m)!\,(2l+1)\,(2-\delta_{0m})}\right]^{\frac{1}{2}} C_{lm} \tag{10}$$

where $\delta_{0m} = 1$ for $m=0$ and $\delta_{0m} = 0$ otherwise.

The $C_{2,0}$ ($-J_2$) coefficient is three orders of magnitude bigger than the next largest coefficient. The magnitude of high order normalized coefficients can be approximated by Kaula's rule of thumb as follows, [*Kaula, 1966, p. 98*].

$$|\bar{C}_{l\,m}| \approx \frac{\sqrt{160} \times 10^{-6}}{\sqrt{2l^4 + l^3}} \approx \frac{10^{-5}}{l^2} \tag{11}$$

Terms with $m = 0$, known as the zonal harmonics, depend only on the geocentric latitude ($\phi$) of the satellite subpoint. General terms, known as tesserals, have both latitude and geocentric longitude ($\lambda$) dependence. For a nearly circular, polar orbit, $\phi$ and $\lambda$ can be approximated by, $\sin\phi = \sin u$, $\lambda = \Omega - \omega_E\, t$.

The following section deals with the $U_{2,0}$ term by itself, followed by a description of the zonal and tesseral effects.

Earth Oblateness

The Earth's equatorial bulge or oblateness has an unnormalized coefficient $C_{2,0} = -J_2 = -1.082 \times 10^{-3}$. We will see in later sections that the coinclination and node will have variations on the order of $10^{-3}$ and that the eccentricity will also be of the same order of magnitude. Thus, $J_2$ will be considered first order small. Substituting $l = 2$, $m = 0$ in Eq 10 gives the $J_2$ potential

$$U_{J2} = -\frac{\mu_E\, J_2\, R_E^2}{a^3 (1 - e^2)^3} (1 + e\cos f)^3 \left( \frac{3}{2} \cos^2 i' \sin^2 u - \frac{1}{2} \right) \tag{12}$$

This expression can be averaged over time to obtain the slowly varying part of the potential. The average $J_2$ potential is then substitued in Eq. 8 to determinethe average rates of the orbit elements. Keeping terms to second order, (i.e. $e^2$, $\eta^2$, $\xi J_2$, $i' J_2$, etc.) we obtain the following nonzero average rates for $\xi$, $\eta$, and $\Omega$, and $u_0$,

$$\begin{aligned}
\frac{d\bar{\xi}_{J2}}{dt} &= \frac{3}{4} n J_2 \frac{R_E^2}{a^2\gamma^4} \eta \\
\frac{d\bar{\eta}_{J2}}{dt} &= -\frac{3}{4} n J_2 \frac{R_E^2}{a^2\gamma^4} \xi \\
\frac{d\bar{\Omega}_{J2}}{dt} &= -\frac{3}{2} n J_2 \frac{R_E^2}{a^2\gamma^4} i' \\
\frac{d\bar{u}_{0\,n}}{dt} &= n \left( 1 - \frac{3}{2} J_2 \frac{R_E^2}{a^2\gamma^3} \right)
\end{aligned} \tag{13}$$

If this were the only disturbance on the orbit, the average eccentricity vector would rotate in the orbit plane at a rate of $6.69 \times 10^{-4}$ rad/orbit (period of 101 days) opposite the orbit motion, and the node would have a secular drift rate of 45.5 $i'$ per year.

Zonal Harmonics

The terms in the spherical expansion of the gravitational field which do not depend on longitude are known as zonal harmonics. The disturbing potential for each zonal term in the model can be expressed as ,

$$U_{l,0} = -\frac{\mu_E R_E^l}{r^{l+1}} J_l \; P_l\,(sin\phi) \tag{14}$$

where $P_l\,(sin\phi) = 2^{-l}\sum_{j=0}^{k} \alpha_{lj}\; sin^{l-2j}\phi$

$$\alpha_{l,j} = \frac{(-1)^{\,j}(2l-2j)!}{j!(l-j)!(l-2j)!},\quad k = \begin{cases} l/2 & for\ l\ even \\ (l-1)/2 & for\ l\ odd \end{cases}$$

For $l$ greater than 2, the average potential over an orbit to first order in $e$ and $i'$ is

$$\begin{aligned} \overline{U}_{l,0} &= -\frac{\mu_E R_E^l\; J_l}{a^{l+1}\,\gamma^{2l-1}}\,\frac{1}{2\pi}\int_0^{2\pi} (1+e\,cos f)^{l-1}\,P_l\,(cos\,i'\,sin\,u)\,du \\ &= -\frac{\mu_E R_E^l\; J_l}{a^{l+1}}\,\frac{1}{2\pi}\int_0^{2\pi} \left[\,1+(l\text{-}1)\,\xi\,cos\,u+(l\text{-}1)\,\eta\,sin\,u\right]\sum_{j=0}^{k}\alpha_{lj}\,sin^{l-2j}u\,du \end{aligned} \tag{15}$$

To first order, the average potential for the even zonals, $J_4$, $J_6$, $J_8$, etc., does not depend on the orbit elements $\xi$, $\eta$, $i'$, or $\Omega$. Thus the average rates of change of the orbit elements are all zero.

For $l$ odd, the average potential has a first order dependence on $\eta$ which produces a constant rate of change of $\xi$, as follows:

$$\frac{d\,\xi_{l\,odd}}{dt} = \sqrt{\frac{\mu_E}{a^3}}\,J_l\,\frac{R_E^l}{a^l}\,(l-1)\,P_{l,1} \tag{16}$$

where $P_{l1} = \sum_{j=0}^{\frac{l-1}{2}} \dfrac{(-1)^{\frac{l-1}{2}-j}(l+2j+1)!}{2^{l+2j+1}\left(\frac{l+1}{2}+j\right)!\left(\frac{l-1}{2}-j\right)!\;j!\,(j+1)!}$

All other average orbit element rates are second order small.

The oscillation in the two components of the eccentricity produced by the Earth oblateness is analogous to a mass-spring system with natural frequency equal to $3/4\; n\, J_2\, R_E^2/\left(a^2\gamma^4\right)$. The rate of change of $\xi$ given in Eq.19 acts like a forcing term which offsets the center of this oscillation. This is equivalent to a constant force acting on a mass-spring system.

The sum of the rates due to the odd harmonics of order 3 to 35 is $0.894 \times 10^{-6}$ per orbit. This rate of change of $\xi$ due to the odd harmonics, divided by the rotation rate of the eccentricity vector due to the Earth oblateness, gives the "frozen eccentricity" offset of 0.001338. The long term motion of the eccentricity vector will be a slow rotation about this offset position.

Tesseral Harmonics Near Resonance

Terms in the gravitational potential given in Eq. 10 for which $m \geq 1$, are known as tesseral harmonics. In general they are a function of both latitude and longitude. Sectoral harmonics, for which $l=m$, depend only on longitude. Kaula [*1966, p.24*] gives the following form for the potential due to a single tesseral of degree $l$ and order $m$ in terms of the spacecraft orbit elements.

$$U_{lm} = \frac{\mu_E}{r}\left(\frac{R_E}{a}\right)^l \sum_{p=0}^{l} \sum_{q=-\infty}^{\infty} F_{lmp}(i)\, G_{lpq}(e)\, J_{lm} \begin{bmatrix} \cos\psi \\ \sin\psi \end{bmatrix}_{l-m\ odd}^{l-m\ even}$$

$$\psi = (l - 2p)\, u_0 + q\, M + m\,(\Omega - \omega_E\, t - \varphi_{lm}) \qquad (17)$$

$$J_{lm} = \sqrt{C_{lm}^2 + S_{lm}^2}\ ,\ \tan(m\varphi_{lm}) = \frac{S_{lm}}{C_{lm}}$$

The inclination function $F_{lmp}$ as expressed by Allan [1967] is,

$$F_{lmp}(i) = \frac{(l+m)!}{2^l\, p!\, (l-p)!} \sum_k (-1)^{k+j} \binom{2l-2p}{k} \binom{2p}{l-m-k} c^{3l-m-2p-2k}\, s^{m-l+2p+2k} \qquad (18)$$

where $c = \cos i/2$, $s = \sin i/2$, $j = 0$ for $l-m$ even and $j = 1$ for $l-m$ odd, and $k$ ranges from $\max(0, l-m-2p)$ to $\min(l-m, 2l-2p)$. The eccentricity function $G_{lpq}$ is a complicated sum which is of order $e^{|q|}$, with $G_{lp0}(e)=1$.

Most tesseral terms will have only short term periodic effects on the orbit elements; however terms which are nearly commensurate with the orbital period may produce large, long term variations in the inclination and node, referred to as librational resonance, and secular growth in the eccentricity and semimajor axis, known as dynamical resonance. Many papers have been written analyzing orbit resonances, and in fact orbital data from near Earth satellites in near resonance have provided the means to estimate certain high order coefficients very accurately [*Allan, 1970, 1971, 1972, etc*]. In the next two sections the effects of the tesseral harmonics on the GP-B orbit plane, and the spacecraft motion within the orbit plane are described.

*Out of Plane Motions*

To investigate the change in the coinclination and node of the orbit due to the tesseral harmonics, set $e=0$, and keep only terms which are first order in $i'$ for the potential in Eq. 12. Substituting this in the variational equations Eq. 8 gives the following expressions for the rate of change of $i'$ and $\Omega$ due to a single term $U_{lm}$.

$$\frac{d\,i'_{lm}}{dt} = n\left(\frac{R_E}{a}\right)^{l} \sum_{p=0}^{l} F_{lmp}\left(\frac{\pi}{2}\right) m\; J_{lm} \begin{bmatrix} -\sin\psi \\ \cos\psi \end{bmatrix}^{l-m\,odd}_{l-m\,even}$$

$$\frac{d\,\Omega_{lm}}{dt} = -\,n\left(\frac{R_E}{a}\right)^{l} \sum_{p=0}^{l} F'_{lmp}\left(\frac{\pi}{2}\right) J_{lm} \begin{bmatrix} \cos\psi \\ \sin\psi \end{bmatrix}^{l-m\,odd}_{l-m\,even} \qquad (19)$$

where $$F'_{lmp}\left(\frac{\pi}{2} - i'\right) \equiv \frac{(l+m)!}{2^{2l}\,p!\,(l-p)!} \sum_{k} (-1)^{k+j} \binom{2l-2p}{k} \binom{2p}{l-m-k} (2l-m-2p-2k)$$

Thus one would expect the coinclination and node to vary sinusoidally unless $\dot{\psi}$ is close to zero. This situation is known as a ***librational*** resonance, where the driving frequency $\dot{\psi}$ associated with a particular harmonic is nearly zero [*Allan, 1967a*]; expressed mathematically as,

$$\dot{\psi} = (\,l - 2\,p\,)\,\dot{u}_0 - m\,\omega_E \approx 0$$

$$\text{or} \quad \dot{\psi} = \alpha\,\dot{u}_0 - \beta\,\omega_E \approx 0 \qquad (20)$$

for some integers $\alpha$ and $\beta$.

For any set of orbit rate and Earth rate multipliers $\alpha$ and $\beta$, we can compute the orbit altitude for which resonance will occur. (For reasonable accuracy in predicting these altitudes the effect of the Earth oblateness must be included in the orbit rate as in Eq. 13.) Table 1 lists the closest resonances for terms up to degree and order 60, for a polar orbit at an altitude of 650 km. The exact resonant altitude and the period of the driving frequency for GP-B associated with these near resonances are also shown.

In general, lower order resonances will be stronger than higher order ones because both the normalized geopotential coefficients and inclination functions slowly decrease as the degree and order increase. That is, although the GP-B orbit is closer to the 44:3 resonance than to 15:1, the latter will probably produce a more substantial variation in the orbit elements.

**Table 1** Near Resonances for Polar 650 km GP-B Orbit .

| $\alpha$ | 2 | 3 | 4 | 1 |
|---|---|---|---|---|
| $\beta$ | 29 | 44 | 59 | 15 |
| Resonant Altitude (km) | 706.5 | 652.6 | 626.1 | 547.9 |
| Period (days) | 2.85 | 40.64 | 3.32 | 3.07 |

Each $\beta/\alpha$ resonance is composed of contributions from a sequence of tesseral terms, which satisfy the conditions $(l\text{-}2p) = \alpha$, and $m = \beta$. For example the lowest order terms in 15/1 resonance are (l,m,p)={(15,15,7), (17,15,8), etc }. Linear analysis can be used to approximate the element rates for these near resonant terms; however, if the computed value for $\dot{\psi}$ is too small, the linear approximations are no longer valid and a more involved

analysis must be performed. In this situation the value of $\dot{\psi}$ may vary considerably and secondary influences must be taken into account.

It is difficult to precisely predict the effects of higher order terms for two reasons. First, the coefficients themselves are not well known and second, the usual series expressions for the inclination function, $F_{lmp}(i)$, such as that given in Eq. 18, require infinite precision for large values of $l$. Recursive [*Kostelecky, 1986*], and FFT methods [*Goad, 1987*] have been developed recently for determining these coefficients reliably; however, these techniques require substantial computational and storage capabilities and were not attempted for this paper.

The work that we have done indicates that the largest variation for GP-B is due to the first few terms in the 15:1 resonance. The simulation results show a $\pm$ 2 x $10^{-5}$ deg variation in the coinclination, and an even smaller oscillation in the node. These variations are small enough to be neglected in the preliminary orbit modeling, but should be included in later studies.

For GP-B we have the flexibility to select the semimajor axis of the orbit so as to avoid low order resonances. Based on these preliminary analyses, it appears that the suggested altitude of 650 km achieves this desired objective. The period of oscillations associated with the 15:1 resonance is three days is fairly short. A long 41 day resonance occurs for $\beta/\alpha$=44/3, which is of high enough order that the effects appear to be negligible for long term orbit modeling purposes. If future work indicates otherwise, the orbit altitude can be adjusted accordingly.

*In-plane Motions*

To investigate the in-plane effects of the tesseral harmonics it is necessary to reintroduce terms in the series expansion of Eq. 17 to first order in $e$. Doing this and substituting the perturbing potential in Eq. 8, gives the following rates for the components of the eccentricity vector [*Allan, 1967b*].

$$\frac{d\,\xi_{lm}}{dt} = n\left(\frac{R_E}{a}\right)^l J_{lm} \sum_{p=0}^{l} F_{lmp}\, G_{lp}^{+} \begin{bmatrix} \cos\psi^{+} \\ \sin\psi^{+} \end{bmatrix}_{l\text{-}m\ odd}^{l\text{-}m\ even} + F_{lmp}\, G_{lp}^{-} \begin{bmatrix} \cos\psi^{-} \\ \sin\psi^{-} \end{bmatrix}_{l\text{-}m\ odd}^{l\text{-}m\ even}$$

$$\frac{d\,\eta_{lm}}{dt} = n\left(\frac{R_E}{a}\right)^l J_{lm} \sum_{p=0}^{l} F_{lmp}\, G_{lp}^{+} \begin{bmatrix} \sin\psi^{+} \\ -\cos\psi^{+} \end{bmatrix}_{l\text{-}m\ odd}^{l\text{-}m\ even} + F_{lmp}\, G_{lp}^{-} \begin{bmatrix} -\sin\psi^{-} \\ -\cos\psi^{-} \end{bmatrix}_{l\text{-}m\ odd}^{l\text{-}m\ even} \tag{21}$$

where $\psi^{\pm} = (l\text{-}2\,p\pm1)\,u_0 + m\,(\Omega - \omega_E)$, $G_{lp}^{+} = \frac{1}{2}(3\,l\text{-}4\,p+1)$, $G_{lp}^{-} = \frac{1}{2}(4\,p - l+1)$

As in the out-of-plane motions, a resonance will occur when $\dot{\psi}$ is near zero. In this case, however, the resonant perturbing force is periodic at the orbital frequency. Blitzer (*1966*) termed these in-plane effects, *dynamical* resonances. Expressed mathematically, the resonant condition is given by [*Allan, 1967b*],

$$\dot{\psi} = ( l - 2p \pm 1 ) \dot{u}_0 - m \omega_E \approx 0$$

$$\text{or} \quad \dot{\psi} = \alpha \dot{u}_0 - \beta \omega_E \approx 0 \tag{22}$$

Thus, the same $\beta/\alpha$ combinations considered for the out-of-plane motions will cause in-plane resonances, but the resonant indices are different (Eq. 20). For each $(l^*,m^*)$ pair there are two resonant values of $p$ corresponding the +1 and -1 values of $q$.

For the 15:1 near resonance,.the eccentricity vector has an amplitude of less than $2 \times 10^{-6}$ and rotates clockwise in the plane with the period of 3.0 days. This variation is insignificant in comparison to the short term changes produced by $J_2$ and does not have a long enough period to cause long term effects as did the odd zonal harmonics. If the spacecraft were in an orbit closer to a low order resonant altitude, tesseral terms could contribute slow or nearly constant offsets to the eccentricity vector which would appear similar to the odd zonal harmonics discussed earlier. Again the higher order tesseral terms in near resonance ($l \geq 44$, and $l \geq 59$) are expected to produce extremely small variations.

## Sun and Moon

The Sun and Moon gravity gradients affect the motion of the spacecraft both directly, and indirectly through the solid Earth tides. The primary gravity gradient effect of each body is a drift consisting of secular and periodic components in the coinclination and node.

The potential due to a distant mass is given by

$$U_B \frac{\mu_B}{|\mathbf{r}_B - \mathbf{r}|} - \frac{\mu_B \, \mathbf{r}_B \cdot \mathbf{r}}{r_B^3} = \frac{\mu_B}{r_B} + \sum_{l=2}^{\infty} \frac{\mu_B \, r^l}{r_B^{l+1}} P_l \left( \mathbf{i}_B \cdot \mathbf{i}_{S/C} \right) \tag{23}$$

where $\mu_B$ is the gravitational constant of the disturbing body, $r_B$ is the distance to the body, and $P_l$ is the Legendre function of the angle between the spacecraft and the disturbing body at the Earth center. $\mathbf{i}_{S/C}$ and $\mathbf{i}_B$ represent unit vectors pointing from the center of the Earth toward the spacecraft and the disturbing body, respectively.

If Eq. 23 is expanded to third order in $\frac{r}{r_B}$, one obtains

$$U_B = \frac{\mu_B}{r_B} + \frac{\mu_B}{r_B} \left( \frac{r}{r_B} \right)^2 \left[ \frac{3}{2} \left( \mathbf{i}_B \cdot \mathbf{i}_{S/C} \right)^2 - \frac{1}{2} \right]$$

$$+ \frac{\mu_B}{r_B} \left( \frac{r}{r_B} \right)^3 \left[ \frac{5}{2} \left( \mathbf{i}_B \cdot \mathbf{i}_{S/C} \right)^3 - \frac{3}{2} \left( \mathbf{i}_B \cdot \mathbf{i}_{S/C} \right) \right] \tag{24}$$

Where the second term in Eq. 24 represents the gravity gradient potential. This perturbing term will have a significant effect on the inclination and node of the orbit. The third term could influence in the in-plane elements; however for GP-B its effect was found to be insignificant.

The gravity gradient potential can be expressed in terms of the right ascension and declination of the perturbing body and the orbital elements of the spacecraft orbit, by making the following substitutions based on Figure 2.10.

$$\mathbf{i}_{S/C} = \cos\phi\ \cos\alpha\ \mathbf{i}_1 + \cos\phi\ \sin\alpha\ \mathbf{i}_2 + \sin\phi\ \mathbf{i}_3$$

$$\mathbf{i}_B = \cos\delta_B\ \cos\alpha_B\ \mathbf{i}_1 + \cos\delta_B\ \sin\alpha_B\ \mathbf{i}_2 + \sin\delta_B\ \mathbf{i}_3 \tag{25}$$

Where for a nearly circular, nearly polar orbit, to first order in $i'$,

$$\alpha = \Omega' + \Delta\alpha, \qquad \sin\phi = \sin u,$$

$$\cos\phi\ \cos\Delta\alpha = \cos u, \qquad \cos\phi\ \sin\Delta\alpha = i'\sin u. \tag{26}$$

Notice that the longitudes, right ascensions, and orbit node ( $\Omega'$) are referred to the direction of the equatorial crossing of the perturbing body ( $\mathbf{i}_1$).

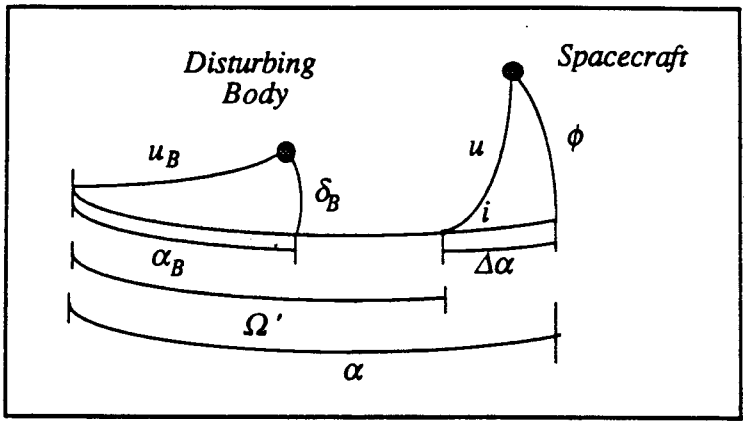


**Fig. 2 Geometry for Disturbing Body (Sun or Moon).**

This gravity gradient potential is averaged over an orbital period and expressed in terms of the position of the disturbing body as follows:

$$\overline{U}_B = \frac{\mu_B a^2}{r_B^3}\left[-\frac{1}{2} + \frac{3}{4}\left(\cos^2(\alpha_B - \Omega')\cos^2\delta_B + \sin^2\delta_B + i'\sin(\alpha_B - \Omega')\sin 2\delta_B\right)\right] \tag{27}$$

Then the average rates of change of $i'$ and $\Omega$ due to the Sun and Moon can be computed from Eq. 8. We find that

$$\frac{d\,\overline{i'}_B}{dt} = \frac{3}{4}\frac{\mu_B}{n\,r_B^3}\sin 2(\alpha_B - \Omega')\cos^2\delta_B$$

$$\frac{d\,\overline{\Omega}_B}{dt} = -\frac{3}{4}\frac{\mu_B}{n\,r_B^3}\sin(\alpha_B - \Omega')\sin 2\delta_B \tag{28}$$

These rates can also be expressed in terms of the argument of latitude, $u_B$, and inclination, $i_B$, of the "orbit" of the perturbing body around the earth, by expanding Eq. 28, and making the following substitutions:

$$\sin \delta_B = \sin i_B \sin u_B$$

$$\cos \delta_B \cos \alpha_B = \cos u_B \qquad (29)$$

$$\cos \delta_B \sin \alpha_B = \cos i_B \sin u_B$$

Then the average rates become

$$\frac{d\bar{i}'_B}{dt} = -\frac{3}{8}\frac{\mu_B}{n r_B^3} \left\{ \sin 2\Omega' \sin^2 i_B \right.$$

$$\left. - 2 \cos 2\Omega' \cos i_B \sin 2u_B + \sin 2\Omega' (1 + \cos^2 i_B) \cos 2u_B \right\} \qquad (30)$$

$$\frac{d\bar{\Omega}_B}{dt} = -\frac{3}{8}\frac{\mu_B}{n r_B^3} \left\{ \sin 2i_B \cos \Omega' \right.$$

$$\left. - \sin 2i_B \cos \Omega' \cos 2u_B - 2 \sin i_B \sin \Omega' \sin 2u_B \right\}$$

The form given in Eq. 30 is particularly useful because it immediately shows that a perturbing body will contribute a secular drift plus a periodic term at twice the rate at which the body orbits the earth. The secular part is simply the first term in each of the expressions above.

Thus, the Sun will cause a secular drift plus a twice yearly oscillation in both coinclination and node. The secular drift is approximately $-1.6 \times 10^{-3}$ deg/yr in coinclination, and $-3.7 \times 10^{-3}$ deg/yr in the right ascension of the node.

The Moon also produces a secular drift plus a twice *monthly* variation; however, the magnitude of the secular term depends on the position of the lunar orbit in its 18.6 year precessional cycle around the ecliptic pole. Fig. 3 shows the motion of the lunar pole with respect to the ecliptic pole and the north pole of the Earth. In the figure the 5 deg cone which the lunar orbit normal traverses about the ecliptic pole is illustrated. Notice that during part of the cycle it just crosses the nominal GP-B orbit plane which is oriented so as to contain the line of sight to Rigel. The orbit plane secular drift rates as a function time during the 18.6 cycle, are shown in Fig. 4.

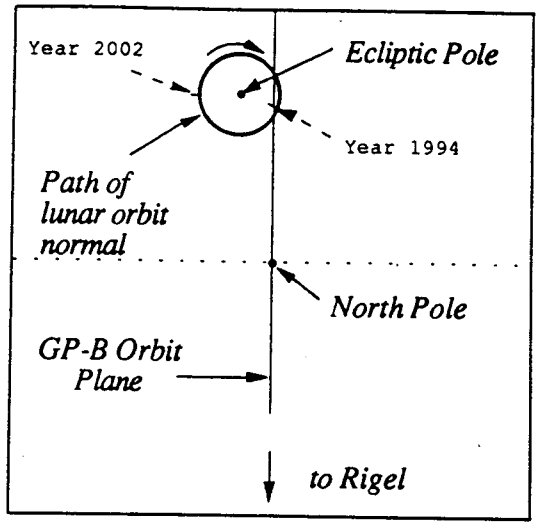


**Fig. 3 Motion of the Lunar Orbit Plane with Respect to the Earth.**

*The top figure shows the relative positions of the Earth's North Pole, the Eliptic Pole and the normal to the lunar orbit plane.*

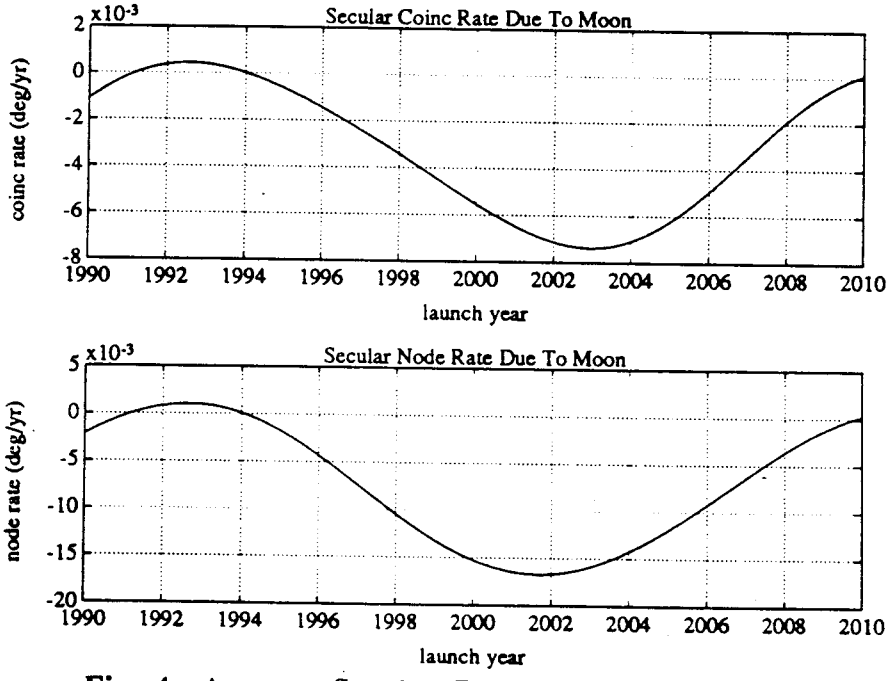


**Fig. 4 Average Secular Rates Due to the Moon.**

Solid Earth Tides

The Sun and Moon exert forces on the Earth which cause variations in its shape. These bulges in turn have a noticeable effect on the orbit of a near Earth satellite. A simple model of this perturbation is often used in which the gravity gradient potential of the Sun or Moon

is evaluated at the surface of the Earth and multiplied by the Love number, $k_2$, and a reduction factor of $\left(\frac{R_E}{r}\right)^3$ [*NASA, 1988, p. 152*].

This formulation was used in the long term simulations for both the Sun and Moon, assuming an elastic response time of zero and a typical Love number $k_2 = 0.3$ [*NASA, 1988, p. 155*]. These secondary effects of the Sun and Moon were found to be less than one fifth of the direct influence. Thus, the simple model seems adequate at this stage of the analysis.

### Precession of the Equinoxes

Precession of the equinoxes refers to the movement of the Earth's spin axis in a 23.5 deg cone about the ecliptic pole. This motion, which is due primarily to the torque exerted by the Sun on the Earth's equatorial bulge, has a period of 25,700 years. As the Earth precesses underneath the spacecraft orbit it produces an effective change in the inclination of the orbit.

The reference point from where the right ascensions of both the guide star and the ascending node of the orbit are normally measured also shifts as a result of the precession of the equinoxes. However, because we are only interested in the relative position of the node relative to Rigel, this shift has no effect on $\Omega$.

The annual general precession is westward at the rate

$$\dot{\psi}_{poe} = \frac{2\pi}{25700\ yr} = 0.000244\ rad/yr = 0.0139\ deg/yr \tag{31}$$

which produces a change in the coinclination of a polar orbit aligned with Rigel of

$$\begin{aligned} \frac{d\, i'_{poe}}{d\, t} &= sin\ (tilt_E)\ sin\ (\lambda_R)\ \dot{\psi}_{poe} \\ &= sin\ (23.5\ deg)\ sin\ (78.484\ deg\ )\ (0.0139\ deg/yr) \\ &= 0.0054\ deg/yr \end{aligned} \tag{32}$$

## LONG TERM ORBIT MOTIONS

Simulation results for the *long term* motions of the spacecraft due to the combined perturbations described in the previous sections will now be presented. By long term we refer to effects which are secular or have periods of more than ten days The expressions for the *orbit averaged* rates of change of the orbit elements were programmed and integrated numerically.

Recall that the objective of the orbit selection is to *maximize the relativity drifts* of the gyros, and to *minimize the Newtonian drifts* of the gyros. Newtonian drifts of the gyro spin axis due to one of the dominant classes of torques are proportional to the angle

between the line of sight to Rigel and the orbit plane, as identified in Eq. 6. Thus the target injection orbit was selected to minimize the maximum separation between the orbit plane and the direction to Rigel, and to reduce the mean eccentricity. The following sections show the orbit evolution and compare the resulting variations in the elements to the requirements described in earlier. The effects of orbit injection errors are also considered. Because of the very low eccentricity of the nominal GP-B orbit and the elimination of nongravitational disturbances by the translational control system, there is no significant coupling between the in-plane and out-of-plane orbit dynamics.

### Out-of-plane Simulation Results

The main contributors to the long term motion of the orbit plane are $J_2$, solar and lunar gravity gradient and tidal effects, and the precession of the equinoxes. In the simulation, the nodal drift due to $J_2$ is modeled according to Eq. 13. The expressions in Eq. 28 for the Sun and Moon effects are used, with the motions of the Sun and Moon modeled based on almanac data [*Naval Observatory, 1985*]. The tides and precession effects are programmed as described. The total orbit average coinclination and node drift rates are integrated numerically over the mission.

Simulations were run for 18 month missions beginning on March 21 for the years 1997 and 2000. Table 2 summarizes the results by giving the target coinclination and node, and the resulting deviations from the nominal orbit. Both the mean and peak values of the coinclination and node are given. The target conditions were selected to minimize the maximum variation in the node over the 18 month mission, because this has the most significant influence in reducing the Newtonian drifts.

**Table 2** Target Values of $i'$ and $\Omega$ for Orbit Injection.
*Initial values and 18 month mean and maximum deviations from the nominal.*

| Start Date | target $i'_0$ (deg) | mean $i'$ (deg) | maximum $\lvert i' \rvert$ (deg) | target $\Omega_0$ (deg) | mean $\Omega$ (deg) | maximum $\lvert \Omega \rvert$ (deg) |
|---|---|---|---|---|---|---|
| Mar. 21, 1997 | 0.00375 | -0.0005 | 0.0057 | -0.0128 | -0.0008 | 0.0187 |
| Mar. 21, 2000 | 0.00640 | -0.0004 | 0.0071 | 0.0260 | -0.0011 | 0.0261 |

The maximum node deviation for the 1997 start date is less than 0.02 deg, and for the year 2000 it is less than 0.03 deg. Fig. 5 illustrates the Newtonian gyro drifts due to the suspension forces for the nominal 1997 and 2000 simulations as modeled by Eq. 6. In

both cases the maximum drift is less than the desired 0.1 marcsec/yr error margin (for at least a 12 month mission).

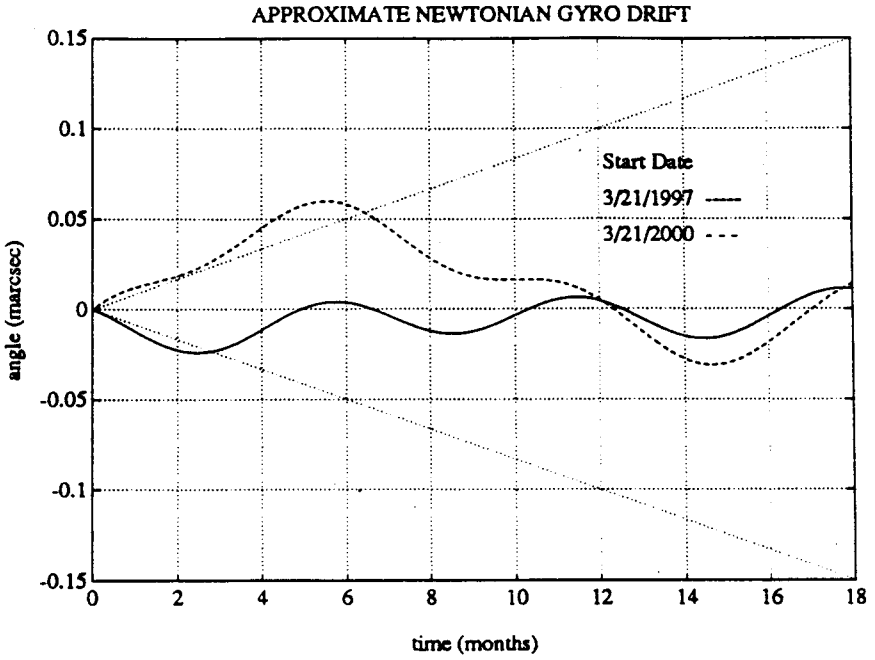


**Fig. 5 Newtonian Gyro Drifts for Nominal Orbit Injection.**

*The solid line shows the drift for nominal conditions in 1997 and the dashed line shows nominal results for the year 2000. The dotted lines indicate the desired drift boundaries of ±0.1 marcsec/yr.*

In order to specify the performance required from the orbit trim system, we must evaluate the effect of orbit injection errors on the long term orbit motion and on the expected gyro drift. Errors in the initial location of the ascending node translate directly into a mean and maximum node error, and have relatively little effect on the coinclination. An initial error of 0.01 deg in the node produces an additional gyro drift of about 0.04 marcsec after 6 months, 0.09 marsec after 1 year, and 0.13 marsec after 1.5 yrs. Thus, one can judge from Fig. 5 that such an error in the node injection can be tolerated in both 1997 and 2000, since the gyro drift remains within 0.1 marcsec for the first twelve months, and within 0.15 marcsec during the full 18 month mission.

Inclination errors have a more subtle effect, due to the $J_2$ induced drift rate which is proportional to the coinclination. Table 3 summarizes the simulation results for initial *coinclination* errors of $\pm 10^{-3}$ deg and $\pm 2 \times 10^{-4}$ deg for each of the launch dates. The evolution of the coinclination and node are plotted in Figs. 6-7. for the target conditions and these initial injection errors.

**Table 3** Mean and Maximum $i'$ and $\Omega$ Due to Inclination Orbit Injection Errors.
*Inclination errors of ± 0.001 and ± 0.0002 for Mar. 1997 and 2000 start dates.*

| Start Date | error $\Delta i'_0$ (deg) | mean $i'$ (deg) | maximum $\lvert i' \rvert$ (deg) | mean $\Omega$ (deg) | maximum $\lvert \Omega \rvert$ (deg) |
|---|---|---|---|---|---|
| Mar. 21, 1997 | -0.0002 | -0.0006 | 0.0059 | +0.0076 | 0.0308 |
| | +0.0002 | -0.0002 | 0.0055 | -0.0060 | 0.0263 |
| | -0.0010 | -0.0014 | 0.0067 | +0.0348 | 0.0794 |
| | +0.0010 | +0.0006 | 0.0057 | -0.0332 | 0.0711 |
| Mar. 21, 2000 | -0.0002 | -0.0006 | 0.0073 | +0.0079 | 0.0381 |
| | +0.0002 | -0.0002 | 0.0069 | -0.0056 | 0.0359 |
| | -0.0010 | -0.0014 | 0.0081 | +0.0350 | 0.0884 |
| | +0.0010 | +0.0006 | 0.0074 | -0.0327 | 0.0751 |

In the coinclination plots one can identify the twice yearly variation due to the solar effect as well as the small twice monthly oscillations caused by the Moon. Notice that in 1997 there is almost no secular drift in the coinclination. In this year the sum of the drift rates produced by the Sun, Moon, $J_2$, and the precession of the equinoxes is almost zero; whereas in the year 2000 there is a net secular drift of about $-4 \times 10^{-3}$ deg/yr in the coinclination. This produces a larger deviation in the node for this year compared to 1997, and causes greater drifts when orbit injection errors occur.

Figs. 8-9 show the Newtonian gyro drifts corresponding to the simulations with inclination injection errors for the 1997 and 2000 start dates, respectively. In both cases, injection errors of ± 0.001 deg (125 m) cause drifts of more than 0.4 marcsec after 18 months. Errors of ± 0.0002 deg (25 m) produce acceptably small gyro drifts, within 0.1 marcsec over the 18 months for the 1997 launch and slightly greater in the year 2000. Clearly this imposes a much tighter injection requirement than the node error. If we allow for a ± 0.0002 deg inclination error, a 0.002 deg node error is still permissible. These results should only be used as a guideline in determining the orbit injection requirements because of the great uncertainty in the actual values of the gyro coefficients and their variability.

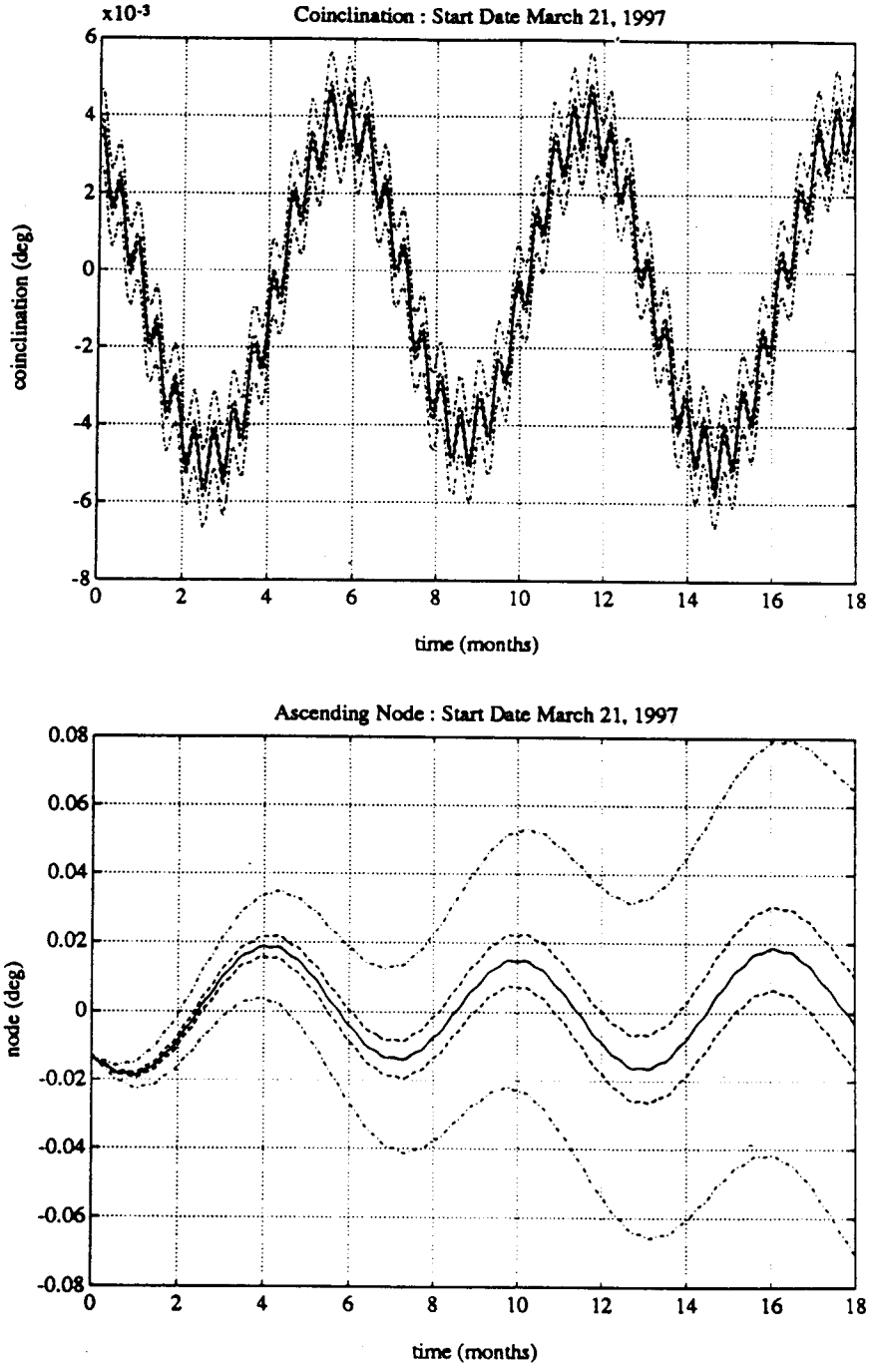


**Fig. 6 Long Term Motion of the Coinclination and Node - March 21, 1997.**

*Solid line shows target orbit evolution. Dashed lines show results for initial coinclination errors of $\pm 2x10^{-4}$ deg. Dash-Dot lines show results for initial coinclination errors of $\pm 10^{-3}$ deg.*

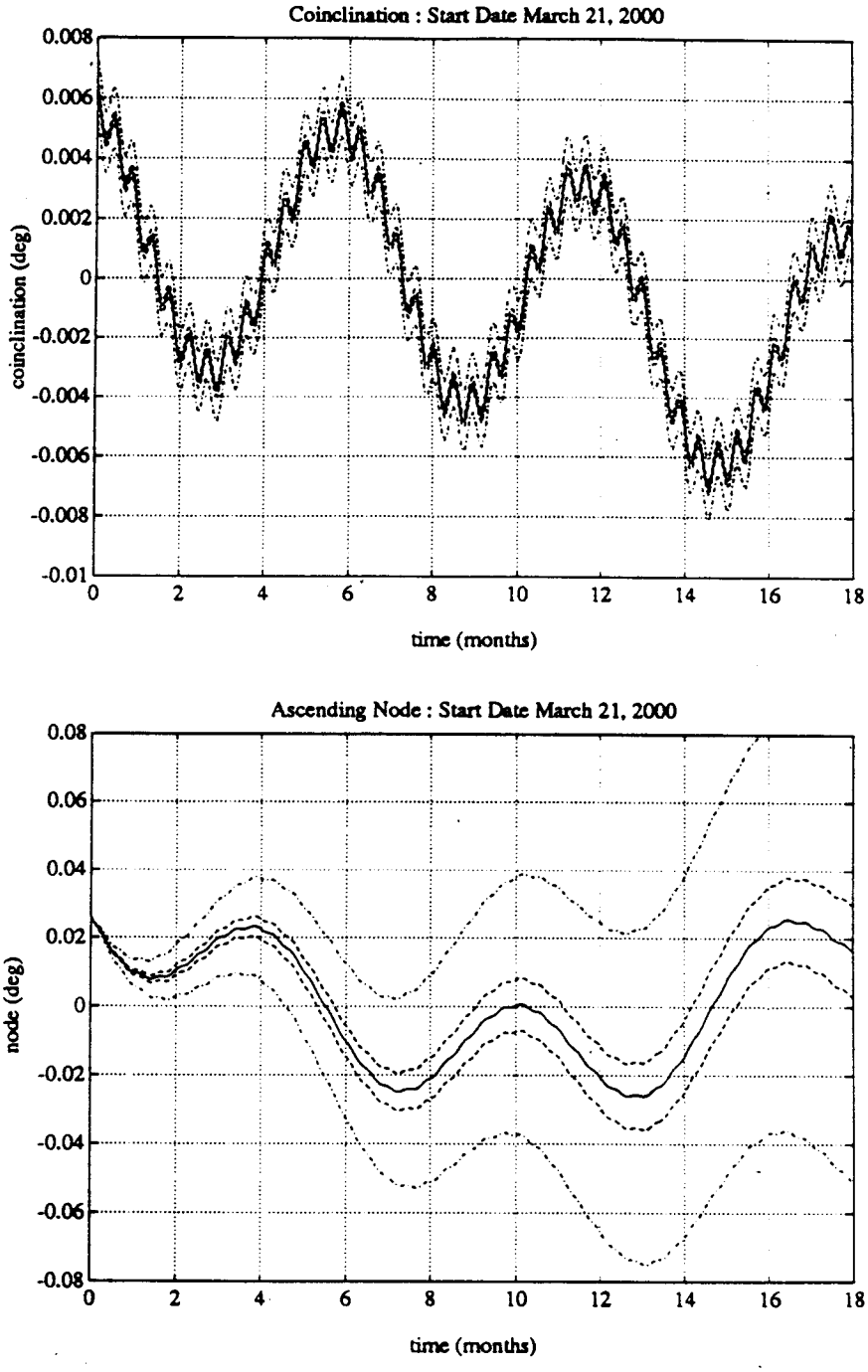


**Fig. 7 Long Term Motion of the Coinclination and Node - March 21, 2000.**

*Solid line shows target orbit evolution. Dashed lines show results for initial coinclination errors of $\pm 2 \times 10^{-4}$ deg. Dash-Dot lines show results for initial coinclination errors of $\pm 10^{-3}$ deg.*

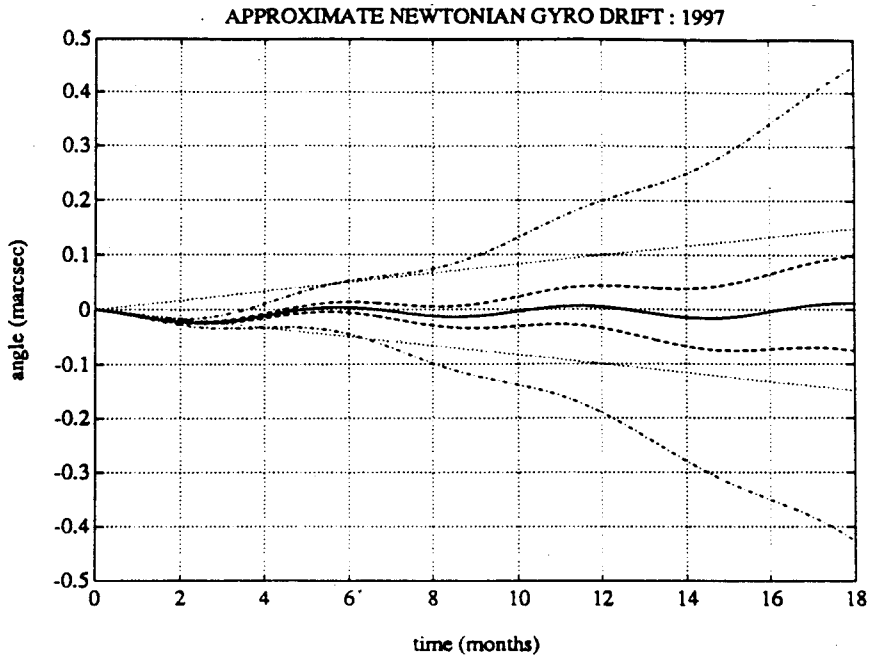


**Fig. 8 Newtonian Gyro Drift - March 21, 1997.**

*Solid line shows target injection. Dashed lines show inclination injection errors of $\pm 2 \times 10^{-4}$ deg. Dash-Dot lines show inclination injection errors of $\pm 10^{-3}$ deg. Dotted lines indicate ±0.1 marsec/yr bounds.*

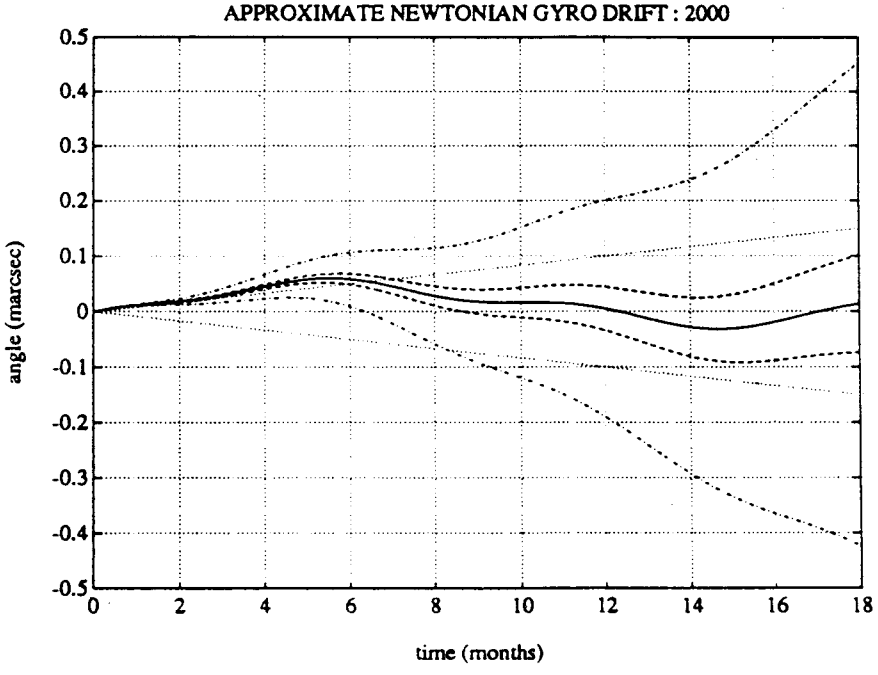


**Fig. 9 Newtonian Gyro Drift - March 21, 2000.**

*Solid line shows target injection., Dashed lines show inclination injection errors of $\pm 2x10^{-4}$ deg. Dash-Dot lines show inclination injection errors of = $\pm 10^{-3}$ deg. Dotted lines indicate ±0.1 marsec/yr bounds.*

### In-Plane Simulation Results

Long term motion within the orbit plane is governed primarily by the Earth oblateness and the odd zonal terms. The near resonant tesseral Earth harmonics and the second order lunar effects were found to cause only neglibly small variations. The $J_2$ term causes the eccentricity vector to rotate in the plane with a period of about 101 days. The constant rate in the equatorial component of the eccentricity produced by the odd zonals changes the center of this rotation from $\xi$=0, $\eta$=0 to $\xi$=0, $\eta$=0.00134. This value of eccentricity, $e$=0.00134, with perigee directed toward the north, is stable for a 650 km polar orbit. For this reason it is known as the frozen eccentricity [*Small, 1986*]. The average eccentricity for GP-B will be minimized by targeting this stable value. Other initial conditions with different eccentricity or with the perigee away from the north pole will eventually cycle to larger eccentricity values.. Fig. 10 shows the trajectory of the eccentricity vector for initial conditions near the frozen value. To ensure that the orbit averaged eccentricity always remains less than 0.002, the initial vector distance from ($\xi_0$,$\eta_0$) to (0,0.00134) must be less than 0.0006.

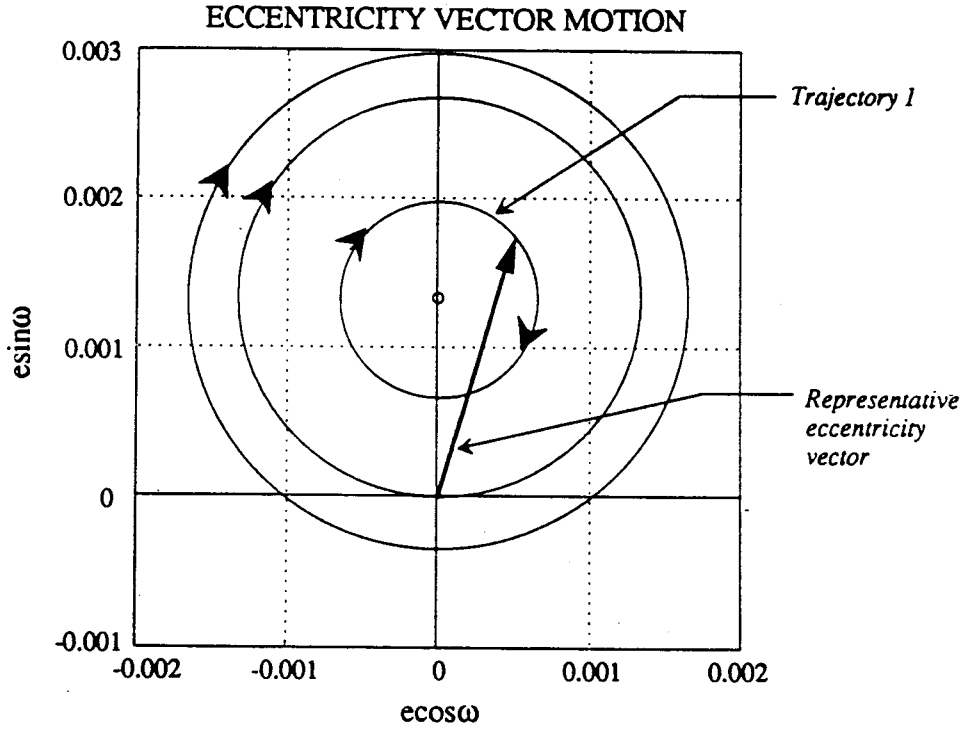


**Fig. 10 Long Term Motion of the Orbit Average Eccentricity Vector.**
*Evolution of the eccentricity vector is shown for four sets of initial conditions. The innermost trajectory is very close to the frozen eccentricity vector of (0.0, 0.00134). Trajectory 1 shows the boundary for the acceptable eccentricity vector errors. Note that if the initial eccentricity is zero it will grow to exceed the permissible value.*

## CONCLUSIONS

The long term orbit averaged motions of the GP-B spacecraft were simulated in order to define a target injection orbit and to review restrictions on how accurately it must be achieved. The target values of the most critical elements- coinclination and ascending node- depend on the experiment start date. Table 3 summarizes the results of this long term study. The *nominal* mission-average values of the orbit elements, the target injection values for candidate start dates in March, 1997 and March, 2000, and acceptable injection errors are given. Out-of-plane requirements are highlighted to emphasize their greater importance. If these conditions are met, the Newtonian drift of the gyro will be less than about 0.1 marcsec and the orbit altitude will not vary by more than 15 km.

The target injection values determined here are *averaged* elements which define the launch vehicle guidance objective. It is unlikely that the upper stage of any booster will be able to meet the stringent requirements specified above; thus there is a critical need for a precise orbit trim system onboard the GP-B spacecraft.

**Table 3 GP-B Orbit Requirements Summary**

| Elements | Nominal Value | Target Injection Value 1997 | Injection Error Magnitude 1997 | Target Injection Value 2000 | Injection Error Magnitude 2000 |
|---|---|---|---|---|---|
| $a$ *(km)* | 7028.14 | 7028.14 | ≤ 5.00 | 7028.14 | ≤ 5.00 |
| $\xi$ | 0.0000 | 0.0000 | ≤ 0.0005 | 0.0000 | ≤ 0.0005 |
| $\eta$ | 0.0000 | 0.0013 | ≤ 0.0005 | 0.0013 | ≤ 0.0005 |
| $i'$ *(deg)* | **0.0000** | **0.00375** | **≤ 0.0002** (≤ 25 m) | **0.00640** | **≤ 0.0002** (≤ 25 m) |
| $\Omega$ *(deg)* *(from Rigel)* | **0.0000** | **-0.0128** | **≤ 0.002** (≤ 250 m) | **0.0260** | **≤ 0.002** (≤ 250 m) |

The results shown in this paper are for two representative launch dates. As the paper goes to publication, the tentative launch date for the GP-B science mission is July 1998. Once a firm launch date has been selected, the analysis and simulations will need to be repeatyed to determine the final orbit injection requirements. A more detailed simulation of the orbit will be needed, including short term effects, to define the final target injection orbit. Standard software packages exist in the industry which can perform the required simulations. This paper is a preliminary analysis of the orbit requirements for the continuinng GP-B mission studies.

## Acknowlegements

The authors wish to thank Dr. Hunt Small of Lockheed for pointing out the stable eccentricity of 0.0013 for a 650 km polar orbit. Also special thanks go to Professor John V. Breakwell of Stanford University for his guidance and useful suggestions throughout this work.

## References

Allan, R. R. (1967a), "Resonance effects due to the longitude dependence of the gravitational field of a rotating primary-I," *Planet. and Space Sciences*, Vol. 15, pp. 53-76.

Allan, R. R. (1967b), "Satellite resonance with longitude-dependent gravity-II; effects involving the eccentricity," *Planetary and Space Sciences*, Vol. 15, pp. 53-76.

Allan, R. R. (1973), "Satellite resonance with longitude-dependent gravity-III; inclination changes for close satellites," *Planet. and Space Sciences*, Vol. 21, pp. 205-225.

Battin, R. H. (1987), *An Introduction to the Mathematics and Methods of Astrodynamics*, New York, AIAA Inc.

Blitzer, L. (1966), "Satellite resonances and librations associated with tesseral harmonics of the geopotential," J. of Geophysical Research, Vol. 71, No. 14, pp3557-3565.

Breakwell, J. V. (1987), Stanford University Class Notes, *Advanced Space Mechanics AA279B*.

Cohen, C. E., G. M. Keiser, and B. W. Parkinson (1990), "Tracking Gravity Probe B gyroscope polhode motion," Reprint from the *Proceedings of the AIAA Guidance, Navigation, and Control Conference*, AIAA Paper 90-3419, Portland.

DeBra, D. B. (1973), "Disturbance compensation system design," APL Technical Digest, **12**, 2, 14-26.

Everitt, C. W. F. (1980), "Report on a program to develop a gyro test of General Relativity in a satellite and associated control technology," Internal report known as *the Green Book*, Stanford University.

Everitt, C. W. F. (1990), Private conversation on October 2, 1990.

Feteih, S. (1989), "Dynamically testing of GP B electrostatically levitated spherical gyroscopes," Ph. D. Dissertation Stanford University, Dept. of Aero. & Astro.

Goad, C. C. (1987), "An efficient algorithm for the evaluation of inclination and eccentricity functions," *Manuscripta Geodaetica*, Vol. 12, No. 1, pp. 11-15.

Kaula, W.H. (1966), *Theory of Satellite Geodesy*, Blaisdell, Waltham, MA.

Kostelecky, J., J. Klokocnik, and Z. Kalina (1986), "Computation of normalized inclination function to high degree for satellites in resonances," *Manuscripta Geodaetica*, Vol. 11, No. 4, pp. 293-304.

Lerch, F. J., et al. (1981),"Goddard Earth models for oceanographic applications (GEM10b and 10c)," *Marine Geodesy*, 5, 2, pp145-187.

NASA Technical Memorandum 4019 (1988), *An Improved Model of the Earth's Gravitational Field: *GEM-T1**.

Naval Observatory (1985), *The Astronomical Almanac*, U.S. Goverment Printing Office, Washington DC.

Parkinson, B. W., C. W. F. Everitt, and D. B. DeBra (1986), "The Stanford Relativity Gyro Experiment," *Guidance and Control, Advances in the Astronautical Sciences*, Vol. 63, AAS.

Parkinson, B. W., et al. (1987), "The prototype design of the Stanford Relativity Gyro Experiment," *38th Congress of the International Astronautical Federation*, Brighton, IAF-87-458.

Small, H. (1986), Lockheed Internal Doc., Question S-B-15, LMSC-F172421.

Vassar, R., et al. (1982a), "Orbit selection for the Stanford Relativity Gyroscope Experiment," *J. of Spacecraft and Rockets*, Vol. 19, No.1, p. 66.

Vassar, R. (1982b), "Error analysis for the Stanford Relativity Gyroscope Experiment," Ph. D. Dissertation Stanford University, Dept. of Aero. & Astro. and Dept. of Physics, SUDAAR No. 531.

Vassar, R. (1986), "Influence of proof mass to gyro spacing on experiment accuracy," LMSC Memorandum #011/F066213.